Protein Dynamics in an Intermediate State of Myoglobin: Optical Absorption, Resonance Raman Spectroscopy, and X-Ray Structure Analysis

Niklas Engler,* Andreas Ostermann,* Alexandra Gassmann,* Don C. Lamb,* Valeri E. Prusakov,† Joachim Schott,‡ Reinhard Schweitzer-Stenner,‡and Fritz G. Parak*

*Physik-Department E17, Technische Universität München, 85747 Garching, Germany; †Institute of Chemical Physics, Russian Academy of Science, Moscow, Russia; and ‡Institut für Experimentelle Physik, Universität Bremen, Germany

ABSTRACT A metastable state of myoglobin is produced by reduction of metmyoglobin at low temperatures. This is done either by irradiation with x-rays at 80 K or by electron transfer from photoexcited tris(2,2′-bipyridine)-ruthenium(II) at 20 K. At temperatures above 150 K, the conformational transition toward the equilibrium deoxymyoglobin is observed. X-ray crystallography, Raman spectroscopy, and temperature-dependent optical absorption spectroscopy show that the metastable state has a six-ligated iron low-spin center. The x-ray structure at 115K proves the similarity of the metastable state with metmyoglobin. The Raman spectra yield the high-frequency vibronic modes and give additional information about the distortion of the heme. Analysis of the temperature dependence of the line shape of the Soret band reveals that a relaxation within the metastable state starts at ~120 K. Parameters representative of static properties of the intermediate state are close to those of CO-ligated myoglobin, while parameters representative of dynamics are close to deoxymyoglobin. Thus within the metastable state the relaxation to the equilibrium is initiated by changes in the dynamic properties of the active site.

INTRODUCTION

Conformational changes in proteins are well known and are necessary for the function of the protein. A typical example is hemoglobin, where the structures of the deoxygenated state and the oxygenated state differ remarkably (Perutz et al., 1998). For a large number of proteins, different conformations have been investigated in detail. Much less is known about the pathway of the relaxation from one conformation to the other. The situation is complicated by the fact that, even within one conformation, the molecules of an ensemble do not have identical structures. As has been shown by the rebinding kinetics of CO-ligated myoglobin (MbCO) after flash photolysis, there are many conformational substates (CSs) (Austin et al., 1975) within a single conformation. CSs differ slightly in structure but may differ in the reaction rates by orders of magnitude. In the case of hemoglobin (Hb) and myoglobin (Mb), the conformation of the protein depends on the ligation state of the heme iron and varies in the structure and the spin state of the iron. The rate at which a protein performs its physiological function is thus restricted by its ability to switch between conformations. The rate of protein function can also depend on the rate of transitions between CS, such as in the rebinding rate of the CO molecule to Mb after flash photolysis (Johnson et al., 1996). During the transition between ligated and unligated Mb and Hb, the enthalpy barrier for rebinding increases. Without this relaxation, ligand rebinding after thermal dissociation would be too fast to allow escape to the solvent (Steinbach et al., 1991).

MbCO has become the model system for investigating conformational substates and the protein relaxations from the ligated to the unligated conformation. The relaxation after photolysis has been investigated in great detail (Agmon and Hopfield, 1983; Steinbach et al., 1991; Lambright et al., 1991; Nienhaus et al., 1992; Balasubramanian et al., 1993; Lim et al., 1993; Franzen and Boxer, 1997; Kleinert et al., 1998; Esquerra et al., 1998). For the characterization of the metastable photodissociated state, Mb*CO, optical absorption spectra have been used (Šrajer et al., 1991; Cupane et al., 1996b). According to these investigations, the active site is not completely relaxed in Mb*CO. Conclusions about structure-function relationships of the CO rebinding can be drawn from a line shape analysis (Ormos et al., 1998), where kinetic hole burning has been observed within Mb*CO and MbCO upon rebinding of the ligand. Because the heme iron is in the plane of the heme in MbCO, it was assumed that the iron displacement from the heme plane is not coupled to the enthalpy barrier for rebinding.

X-ray analysis has yielded structural information about the intermediate state after photodissociation. At low temperature, a metastable state has been observed where the ligand is photodissociated within the heme pocket (Teng et al., 1994; Schlichting et al., 1994; Hartmann et al., 1996). This intermediate state is also observed transiently at room temperature (Šrajer et al., 1996), and a careful theoretical analysis of the intermediate state has been performed (Vitkup et al., 1997).

To investigate the general process of protein relaxation from a nonequilibrium state to its equilibrium state, we involve a different type of experiment (Parak and Prusakov, 1994; Prusakov et al., 1995). A nonequilibrium state is

Received for publication 14 June 1999 and in final form 6 January 2000.

Address reprint requests to Dr. Fritz G. Parak, Physik-Department E17, Technische Universität München, D-85747 Garching, Germany. Tel.: +49-89-289-12551; Fax: +49-89-289-12548. E-mail: fritz.parak@ph.tum.de.

0006-3495/00/04/2081/12 $2.00

produced by reduction of metmyoglobin (metMb) at 80 K. The structure at this temperature is metastable and cannot relax into the equilibrium deoxymyoglobin (deoxyMb) structure, although the iron has changed its electronic configuration. The state has been characterized by Mössbauer spectroscopy (Prusakov et al., 1995). The iron is in a 2+ low-spin state, with the water molecule still bound as the sixth ligand (Fe(II)MbH_2O). As has been shown by Lamb et al. (1998b), the water molecule can be photodissociated and even rebinds at temperatures below 150 K. The rebinding kinetics have been measured and interpreted in terms of a distribution of enthalpy barriers similar to those for MbCO and MbO_2. As the temperature is raised above 150 K, the protein relaxes to the deoxyMb conformation, the water ligand is lost, and the iron moves to the deoxy position. This motion is accompanied by a spin change of the iron from low to high spin (Prusakov et al., 1995).

In this publication we employ a number of techniques to get more detailed information on the static and dynamic properties of the Fe(II)MbH_2O state. First of all, the structure has been investigated at 115K. To investigate the dynamic properties of the Fe(II)MbH_2O state, we measured the temperature dependence of the Soret band below 190 K and analyzed its band shape and temperature dependence in terms of the vibronic theory as described by Cupane et al. (1995). This approach explicitly considers the vibronic coupling of the totally symmetrical heme vibrations with frequencies extracted from resonance Raman spectroscopy and the coupling with thermally populated low-frequency modes (Šrajer et al., 1986) to the electronic transition. This analysis provides information on the vibronic coupling strength of the high-frequency heme vibrations, the coupling to the bath of low-frequency modes, and the inhomogeneous broadening caused by conformational heterogeneity. The vibronic coupling constants of the heme vibrations were also determined from the band intensities of resonance Raman spectra taken with Soret excitation (413 nm) to check the validity of the Soret band analysis. Moreover, resonance Raman spectra taken with different excitation wavelengths in the Q- and B-band regions were utilized to characterize the spin and ligation state of the heme iron and allowed us to identify the origin of an asymmetrical distortion of the heme.

MATERIALS, METHODS, AND DATA EVALUATION

X-ray structure determination

A sperm whale metMb crystal in the space group $P2_1$ containing ^{57}Fe-enriched Mb was irradiated by x-rays for 70 h at 90 K. The irradiation source was a copper x-ray tube without monochromator running at 40 kV and 30 mA. The successful reduction of the crystal was verified by Mössbauer spectroscopy. An x-ray structure determination of the irradiated crystal was performed at 115 K under a flow of cold nitrogen. As a reference, the structure of an unirradiated metMb crystal from the same crystallization batch was determined at the same temperature. Reflection intensities were collected on an Enraf Nonius FR591 rotating anode, using a Siemens Histar multiwire proportional counter mounted on a three-circle diffractometer.

The intensities of the reflections were integrated and scaled by the program SAINT (Siemens). Subsequent data reduction was performed by the CCP4 programs AGROVATA and TRUNCATE (CCP4, 1994). The refinement was done using the program X-PLOR 3.1 (Brünger, 1992). The structure of metMb at 115 K (Parak et al., 1987) was used as the starting model. For both structure refinements, the position of the water molecule that coordinates the heme iron was not restrained to the iron or any other part of the molecule, neither by bonded nor by nonbonded interaction. No angle restraints were used for the proximal histidine with respect to the iron atom. The bond restraints for the proximal histidine bond as well as for the pyrrole nitrogen bonds to the iron were weakened from the standard X-PLOR values to allow an almost unrestrained refinement of this region (Table 1). The positions of the active-site atoms in the final models were verified by calculated simulated annealing omit maps (Hodel et al., 1992).

Resonance Raman measurements

For these experiments, it was important to obtain a sample with a high concentration of intermediate state and very few impurities. Freeze-dried sperm whale myoglobin (Sigma Chemical Co., St. Louis, MO) was dissolved in sodium phosphate buffer at pH 6.0 and purified using both cation exchange and a gel permeation (potassium phosphate buffer, pH 6.6). The purified sample was concentrated and diluted in a buffer/glycerol mixture to yield a final concentration of 500 μM Mb in 50 mM potassium phosphate with 75% glycerol (v/v) at pH 6.6. The sample was loaded in a 2-mm-thick sample cell between two mylar windows and mounted in a small cryostat with beryllium windows. The sample was reduced by x-rays as in the case of the x-ray structure analysis. It was illuminated for 12 h on each side. By illumination, color centers are generated with a peak absorption around 560 nm. To remove these centers, the sample was warmed to 150 K for 10 h.

For the Raman measurements, the mylar window was removed from one side of the sample at 77 K before being loaded into a glass dewar filled with liquid N_2. The instrumentation used for the (nonresonance) Raman experiments is described by Jentzen et al. (1995). The polarized Raman spectra were excited at 413 nm, 520 nm, and 568 nm by a krypton ion laser (Coherent, Innova 90 K) and at 442 nm by a HeCd laser (Omnichromne, Cinho, CA). We used a backscattering geometry with a polarization analyzer followed by a scrambler between the collimator and the entrance slit of the spectrometer to measure the Raman intensity of the two components polarized parallel and perpendicular to the polarization of the incident laser beam. The incident laser beam was polarized perpendicular to the scattering plane. All spectra were recorded with a CCD camera and stored on a PC for further analysis. The spectral slit function of the spectrometer was determined by recording the spectral lines of several pencil lamps (xenon, krypton, etc.) to deconvolute the spectrometer slit function from the measured band shapes of the heme spectra. The frequency positions of these spectral lines were used for calibrating the spectra, so that that the line position could be determined with an accuracy of $\sim$0.2 cm^{-1}. The spectral resolution varied between 2.5 cm^{-1} (with 413-nm excitation) and 1 cm^{-1} (with 568-nm excitation).

A novel lineshape analysis program called MULTIFIT was employed to identify the frequency positions, line profiles, and linewidths (full widths at half-maximum) of all Raman lines. The Raman lines were fitted with a convolution of a line profile (Lorentzian or Gaussian) and the spectrometer's transfer function. Ambiguities were eliminated in the lineshape analysis by using the same frequency, half-width, and lineshape to fit each Raman line for all excitation wavelengths. Thus a self-consistent global fit of all measured spectra was obtained; only the line intensities were used as fitting parameters. The background intensity has been taken into account by either a linear function or a second-order polynomial. All spectra were

TABLE 1 Data collection and refinement statistics

	met Mb	Fe(II)MbH$_2$O
Data collection		
Space group	$P2_1$	$P2_1$
Unit cell (Å) (°)	$a = 63.98$, $b = 30.75$, $c = 34.35$ $\beta = 105.7$	$a = 63.98$, $b = 30.75$, $c = 34.35$ $\beta = 105.7$
Resolution (Å)	10.0 − 1.5	10.0 − 1.4
Measured reflections	86451	91494
$\langle I\rangle/\langle\sigma(I)\rangle$	11.8 (8.2)	10.7 (7.1)
Unique reflections	19721	23704
Completeness overall (%)	94.7 (75.7)	92.8 (80.3)
R_{merge} (%)	4.0	4.3
Temperature (K)	115	115
Refinement		
Resolution range	7.0 − 1.5	7.0 − 1.4
No. of reflections	19565	23550
Working set/test set	17590/1975	21162/2388
R_{cryst} (%)	17.6	17.7
R_{free} (%)	20.8	20.0
r.m.s.d. of bond length (Å)	0.008	0.008
r.m.s.d. of bond angles (°)	1.1	1.1
r.m.s. coordinate error (Å)	0.13	0.11
Geometry		
Fe-H$_2$O (Å)	2.23	2.13
Fe-His93 (Å)	2.15	2.08
Fe-⟨heme plane⟩ (Å)	0.13	0.15
Fe-N$_{plane}$ (Å)	0.08	0.08

Values in parentheses refer to the highest resolution shell, 1.55 − 1.5 Å for met Mb and 1.45 − 1.4 Å for Fe(II)MbH$_2$O. $R_{merge} = \Sigma_{hkl}\Sigma_j|I_j - \langle I\rangle|/\Sigma_{hkl}\Sigma_j\langle I\rangle$, where I_j is the intensity I for the jth measurement of the reflection with indices hkl and $\langle I\rangle$ is the mean of all measurements of the reflection I. $R_{cryst} = \Sigma_{hkl}|F^o_{hkl} - F^c_{hkl}|/\Sigma_{hkl}|F^o_{hkl}|$, where F^c_{hkl} and F^o_{hkl} are the observed and calculated structure factor amplitudes for the reflection hkl. R_{free} is the crystallographic R value calculated with the structure factor amplitudes of the test set which is not involved in the refinement calculations. The given overall coordinate error was estimated by a σ_A plot (Read, 1986). For the calculation of the Fe-⟨heme plane⟩ and Fe-⟨N$_{plane}$⟩ distances, the planes are defined as the best-fit planes through the 20 central C-atoms of the heme and the four heme N-atoms, respectively.

corrected for self-absorption. The line areas were used as a measure of the relative intensities. By measuring all spectra polarized parallel ($I_\parallel$) and perpendicular ($I_\perp$) to the polarization of the exciting laser beam, we were able to calculate the depolarization ratio: $\rho = I_\perp/I_\parallel$. For an unperturbed D_{4h} symmetry, ρ equals 0.125 for A_{1g}, 0.75 for B_{1g} and B_{2g}, and ∞ for A_{2g}-modes (Spiro, 1983). Symmetry lowering may cause deviations from these values and a dispersion of the depolarization ratio (Zgierski and Pawlikowski, 1982; Schweitzer-Stenner, 1989). Details of the theory for the determination of the vibronic coupling parameters have been described by Schweitzer-Stenner et al. (1997). It comprises full consideration of intra- and intermanifold coupling between the lowest vibronic Q- and B-states. Here we consider solely B-state excitation and confine ourselves to the more intense A_{1g}-type modes. This formalism does not consider the occurrence of asymmetrical distortions that have a strong impact on the heme group of Fe(II)MbH$_2$O. We could not determine the depolarization ratio with high precision because of the optical quality of the x-ray-reduced sample. Hence we could explicitly take into account the contributions of vibronic distortions in the Raman tensor (Schweitzer-Stenner, 1989). Therefore, the formalism for the Raman tensor is only evaluated for A_{1g} modes, and the matrix elements are evaluated only for the B_x and B_y states. No mixing with the Q_x and Q_y states is considered. The fit to the resonance excitation and the depolarization ratios of ν_2, ν_4, ν_7, and ν_8 was performed in a similar way, as described in Schweitzer-Stenner et al. (1997). Only the coupling constants for the corresponding A_{1g} modes were used as free parameters to evaluate the first-order terms in the Raman tensor. Then the obtained coupling parameters were scaled by a factor and inserted into the third-order terms in the Raman tensor describing multimode mixing. The scaling factor was adjusted to optimize the mixing of third- and first-order terms. The A_{1g} coupling parameters $(c_{BB}^{A1g})_{hj}$ obtained from the Raman spectra were converted by

$$S_{hj} = \left(\frac{(c_{BB}^{A_{1g}})_{hj}}{\nu_{hj}}\right)^2, \quad (1)$$

to compare them to the coupling constants S_{hj} obtained from the fit of the lineshape of the Soret band (Cupane et al., 1996a). The frequency of the mode is denoted by ν_{hj}.

Optical absorption measurements

We used a solvent of 25% (v/v) water and 75% (v/v) glycerol (Fluka Chemie AG, Buchs, Switzerland) containing 50 mM potassium phosphate buffer. The high concentration of glycerol allowed us to prepare thin, optically transparent samples at low temperature. We used tris(2,2′-bipyridine)ruthenium(II) chloride ($[Ru(bpy)_3]^{2+}$) as a photoactivated reducing agent. Sample 1 (S1) contained 5 mM sperm whale Mb (Sigma), together with 100 mM EDTA (Sigma), and 60 mM $[Ru(bpy)_3]^{2+}$ (Fluka) in the solvent with a final pH value of 6.6. Details of the preparation are given by Lamb et al. (1998a). For the deconvolution of the spectra obtained from sample 1, a number of reference samples had to be measured. Sample 2 (S2 metMb) was obtained by dissolving pure metMb in the solute. For sample 3 (S3 deoxyMb), metMb was dissolved in the solvent and reduced with sodium dithionite (Sigma) under anaerobic conditions. Sample 4 (S4 Ru)

contained pure $[Ru(bpy)_3]^{2+}$ in the solute, and sample 5 (S5 sol) was the solvent alone.

The spectra from 320 nm to 750 nm were acquired with the same equipment as described in Lamb et al. (1998a).

We first cooled sample S1 to 20 K and measured spectra from 20 K to 200 K in steps of 10 K (spectra called S1 metMb). Afterward, the sample was cooled again to 20 K and reduced by laser flashes. The sample was illuminated at 460 nm by 1.2-μs pulses of 33-mJ energy at a repetition rate of 1 Hz. After illumination, 42% of the molecules were reduced. The sample was then warmed to 100 K and kept at this temperature for 15 min to allow the rebinding of any photodissociated water (Lamb et al., 1998b) and to allow additional reduction by trapped electrons. The sample was cooled to 20 K again (now called S1 Mbint150), and spectra have been measured in steps of 10 K up to 150 K. The sample was kept at 150 K for 320 min before cooling to 20 K again. Three further temperature cycles with increasing final temperatures were taken, always starting at 20 K and with final temperatures of 170 K (sample S1 Mbint170), 180 K (sample S1 Mbint180), and 200 K (S1 Mbint200), respectively. Finally the sample was warmed to 295 K and completely reduced by two flashes of 33 mJ. With this sample (called S1 deoxyMb), the temperature-dependent spectra of the fully reduced sample (deoxyMb) were measured.

Reference spectra of the $[Ru(bpy)_3]^{2+}$ sample, S4 Ru, were measured according to the same protocol described above. For the samples S2 metMb, S3 deoxyMb, and S5 sol, only one temperature series was performed from 20 K to 200 K.

After reduction the spectra at low temperature are a superposition of the intermediate state with contributions of $[Ru(bpy)_3]^{2+}$, metMb, and, sometimes, deoxyMb. Reference spectra of Mb with $[Ru(bpy)_3]^{2+}$ were collected because the Soret band of metMb shifts by 0.5 nm upon the addition of 50 mM $[Ru(bpy)_3]^{2+}$ (sample S1 metMb). Because we measured the complete temperature cycle with all reference samples, we can always compare spectra at the same temperature. In the first step, the pure solute spectra (sample S5 sol) are subtracted from all other spectra, and the average absorption between 700 nm and 750 nm was shifted to 0 ODs. The second step is to subtract the correct amount of $[Ru(bpy)_3]^{2+}$ from the metMb (S1 metMb), deoxyMb (S1 deoxyMb), and intermediate state spectra (sample S1 Mbint). The $[Ru(bpy)_3]^{2+}$ concentrations in the metMb and deoxyMb samples were determined by fitting S1 metMb and S1 deoxyMb with pure spectra of $[Ru(bpy)_3]^{2+}$ (S4 Ru) and either pure metMb (S2 metMb) or pure deoxyMb (S3 deoxyMb) spectra. Because S1 metMb and S1 deoxyMb are essentially the same sample, the $[Ru(bpy)_3]^{2+}$ content should be the same. However, the $[Ru(bpy)_3]^{2+}$ concentration from S1 deoxyMb spectra was slightly less ($\sim$5%) than that from the S1 metMb spectra. The small difference can be attributed to photobleaching of the $[Ru(bpy)_3]^{2+}$. To subtract $[Ru(bpy)_3]^{2+}$ from the intermediate state spectra, S1 Mbint, the effect of photobleaching was taken into account by using the average of the two $[Ru(bpy)_3]^{2+}$ concentrations.

After the Ru absorption has been removed from the spectra of S1 Mbmet, S1 deoxyMb, and S1 Mbint, the next step is to subtract the metMb contribution from the partially reduced intermediate state spectra of S1 Mbint. We used the charge transfer band of metMb at 630 nm (15,870 cm^{-1}; Makinen and Churg, 1983) to determine the amount of unreduced myoglobin. Below 170 K, no additional conversion of metMb is observed compared to the starting point at 20 K. The amount of metMb fit to the intermediate state spectra is therefore averaged over the first three temperature cycles up to the temperature of 170 K. In this way, the deconvolution of spectra of the samples S1 Mbint150, S1 Mbint170, and S1 Mbint180 up to 170 K is finished. In the third cycle the temperature of 170 K is exceeded, and additional reduction of metMb occurs by electrons that have been trapped. For the 180 K spectrum of the third cycle, the averaged metMb concentration of the fourth temperature series is used.

The last step that remains is the correction for any protein that has totally relaxed to the deoxyMb state. Relaxation to deoxyMb is only observable above 150 K: therefore, only the spectra of S1 Mbint170 above 150 K and S1 Mbint180 have to be corrected for deoxyMb absorption. To determine the deoxyMb content, each spectrum is fit by a superposition of an intermediate-state spectrum from the previous temperature series (or the previous temperature if there was no earlier measurement at that temperature) and a deoxyMb spectrum. The total protein concentration is held constant.

Fig. 1 *A* shows a typical deconvolution of the intermediate-state spectrum. Even using the procedure described above, we observe contamination of the intermediate-state spectra by absorption of $[Ru(bpy)_3]^{2+}$ and deoxyMb on the red edge of the Soret band (Fig. 4 *B*). The Soret band of deoxyMb is shifted substantially ($\sim$3 nm). The shift is decreasing systematically toward the equilibrium position with increasing relaxation. The deoxyMb absorption limits the resolution of the red edge of the Soret band of the Fe(II)MbH_2O. The influence of the ruthenium contamination on the further analysis of the spectra is small because it is well separated from the Soret band.

The Soret band of myoglobin arises from a $\pi \rightarrow \pi^*$ transition of the porphyrin ring and is sensitive to the charge, spin, and ligation state of the heme iron (Makinen and Churg, 1983). Moreover, it is very sensitive to temperature changes. A rise in the temperature results in an increase in the linewidth, a decrease in the integrated intensity, and a shift of the peak frequency. The physical reason for these effects is the coupling of the electronic transition responsible for the absorption band with the thermal

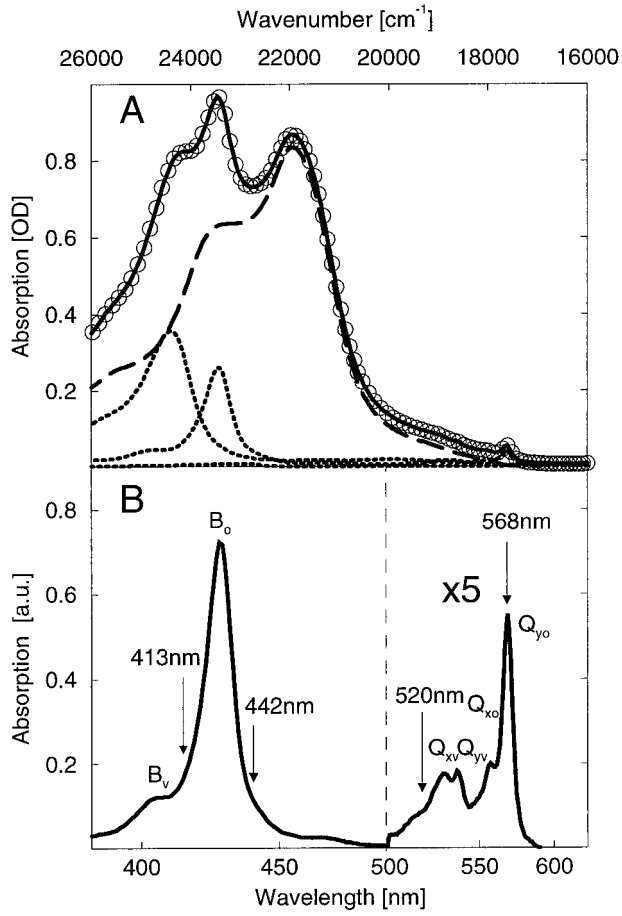

FIGURE 1 (*A*) *Circles*: A typical spectrum measured during the third temperature cycle at 150 K. *Lines*: Deconvolution into the different species. *Dashed line*: Ru contribution. *Dotted lines*: Myoglobin contributions. *Solid line*: Sum of all contributions. (*B*) Optical spectrum of the intermediate state. *Arrows*: Excitation wavelengths used for the Raman experiments. The *x* axis is given in wavenumbers (*top scale*) and wavelengths (*bottom axis*), respectively.

vibrations of the atoms nearby. An analysis of the temperature-dependent spectra gives information on the dynamic properties of the protein in the region of the chromophore.

To get an expression that can be handled analytically, one assumes that the thermal vibrations of the atoms surrounding the iron can be divided into two different types of vibrational modes: the so-called high-frequency vibrational modes and the low-frequency vibrational modes. High-frequency vibrational modes are defined as modes where the electronic transitions occur predominantly from the zeroth vibrational state of the electronic ground state. In other words, the corresponding vibrational energy of these modes is much larger than the thermal energy, $h\nu_h \gg k_BT$ (the index h refers to high frequency). In contrast, the higher states of the low-frequency vibrational modes are significantly occupied within the electronic ground state, because $h\nu_l \leq k_BT$ (the index l refers to low frequency). This means that electronic transitions coupled to low-frequency modes occur from different vibrational states of the electronic ground state. Thus for low-frequency modes both absorption and emission of phonons are possible. High-frequency modes lead to absorption bands in the spectra shifted to higher energies as compared to the pure electronic transition. The low-frequency modes lead to a broadening of these bands, which is shown to be Gaussian within the short time approximation by Chan and Page (1983, 1984). The theoretical description of the electronic-vibrations coupling has led to an analytical expression suitable for fitting the optical absorption spectra in the frequency domain over the entire temperature range measured (DiPace et al., 1992; Cupane et al., 1995). The optical absorption coefficient, $\mu(\nu)$, can be written as a Gaussian distribution, $G(\nu)$, of Lorentzians, $L(\nu)$:

$$\mu(\nu) = M \cdot \nu \cdot \{L(\nu) \otimes G(\nu)\}, \tag{2}$$

where M is a constant that is used to normalize theoretical and experimental values and ν is the absorption frequency. The symbol $\otimes$ signifies the convolution operator. Writing Eq. 2 more explicitly, one obtains the following expression for the Lorentzian function:

$$L(\nu) = \sum_{m_{h1}, m_{h2}, \ldots, m_{hN}} \left[\prod_{j=1}^{N} \frac{(S_{hj})^{m_{hj}} \cdot e^{-S_{hj}}}{m_{hj}!} \right] \cdot \frac{\Gamma}{[\nu - \nu_0(T) - \sum_{j=1}^{N} m_{hj} R_{hj} \nu_{hj}]^2 + \Gamma^2} \cdot \tag{3}$$

Neglecting for a moment all vibrational modes, Eq. 3 describes essentially a Lorentzian of width Γ, determined by the lifetime of the excited state and centered at the temperature-dependent frequency $\nu_0(T)$. The high-frequency vibrational modes j shift this frequency, depending on the frequency of the mode, ν_{hj}, its vibrational quantum number, m_{hj}, and the quadratic coupling constant R_{hj}. The quadratic coupling constant takes into account the change in the vibrational frequencies from the ground state to the excited state. The weight factor for the contribution of the different high-frequency vibrational modes contains the linear coupling constants S_{hj}. They are a measure of the coupling of the vibrational mode with frequency ν_{hj} to the electronic transition and the shift of the nucleus equilibrium position upon excitation. The temperature dependence of the transition frequency $\nu_0(T)$ is caused by the coupling to the low-frequency modes. But in the nonequilibrium case investigated here, we have to consider the strong additional shift of the peak frequency due to the relaxation within the intermediate state. The intrinsic temperature dependence is typically a few cm^{-1} (DiPace et al., 1992), whereas the relaxation leads to a shift of 100 cm^{-1}.

The high-frequency vibrational modes can be resolved individually by resonance Raman spectroscopy. In our case, the coupling parameters of five modes ($N = 5$), which appear with comparatively strong intensity in the resonance Raman spectra obtained with Soret excitation, were explicitly considered in the absorption band analysis. We have used four totally symmetrical modes from the Raman spectra: modes ν_8 at 372 cm^{-1}, ν_7 at 673 cm^{-1}, ν_4 at 1362 cm^{-1}, and ν_2 at 1605 cm^{-1} (the corresponding nomenclature for Eq. 3 is ν_{h1}, ν_{h2}, ν_{h4}, ν_{h5}). In addition, we use a mode at 1000 cm^{-1} (called ν_{h3}), which accounts for the near-lying modes in this region. In the summation, m_{hj} ran from 0 to 2 for each high-frequency mode, which means that transitions involving the creation of three and more vibrational quanta were neglected. The quadratic coupling, R_{hj}, was set equal to 1.

The low-frequency modes are taken into account by line broadening with a Gaussian distribution with the width $\sigma(T)$:

$$G(\nu) = \frac{1}{\sigma(T)} e^{-\nu^2/2\sigma(T)}, \tag{4}$$

where $\sigma(T)$ depends upon the coupling of the electronic transition to low-frequency vibrational modes. $\sigma(T)$ consists of two additive parts, one that reflects the increasing population of low-frequency modes with temperature, and a temperature-independent part, which describes the distribution of the electronic transition frequency by the distribution of conformational substates. In our discussion we focus only on the temperature-dependent part.

In addition to the strong electronic transition vibronic structure on the blue edge, the spectra show a higher wavelength N band. The N band is modeled as a Gaussian band with fixed position at 29,000 cm^{-1} and a width of 2045 cm^{-1}.

RESULTS

X-ray structure analysis

The structure determination of the intermediate state Mbint ≡ Fe(II)MbH$_2$O shows that the reduction of the iron in metMb at 90 K does not change the structure significantly (Table 1 and Fig. 2). At low temperature, no structural relaxation into the deoxyMb equilibrium structure is ob-

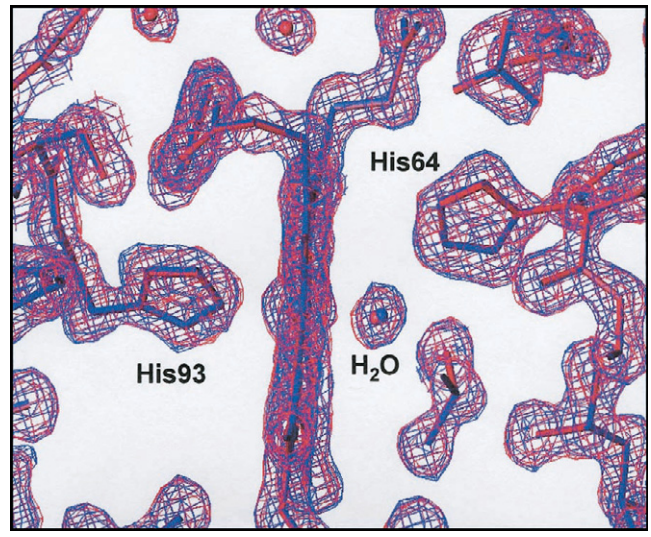

FIGURE 2 The x-ray structure of metMb (*blue*) and the intermediate state (*red*) at 115K. $(2F^o - F^c_{omit})\exp(i\varphi^c_{omit})$ omit electron density maps of metMb (*blue*) and the intermediate (*red*) are contoured at 1.5 of the standard deviation. For the map calculations the iron atom, the proximal histidine, and the water molecule that coordinates the iron were omitted for the calculation of F^c_{omit} and φ^c_{omit}.

served. The electron density at the sixth coordination clearly proves that the water molecule that occupies this position in metMb is still present with full occupancy. However, it cannot be excluded that the water became an OH^-.

Resonance Raman spectra

Fig. 1 *B* shows the optical absorption spectrum of the intermediate Fe(II)MbH_2O measured at 77 K. For the sake of clarity, only unpolarized spectra are shown in the upper two panels of Fig. 3, whereas the lower panel displays the polarized spectra taken with 568-nm excitation. The spectral analysis was done with the polarized spectra. The frequencies and depolarization ratios of the most relevant Raman bands and their mode assignments are listed in Table 2. The mode assignment was done on the basis of normal coordinate calculations on the classical model substance Ni(II)-octaethylporphyrin (Li et al., 1990) and more recent work on hemes in various heme proteins (Smulevich et al., 1996; Hu et al., 1996).

Fig. 3 *A* shows the spectrum taken at 413 nm. With this excitation wavelength, one predominantly enhances modes that exhibit A_{1g} symmetry in D_{4h} (i.e., ν_2, ν_3, and ν_7). The intensity of ν_8 appears comparatively weak. Fig. 3 *B* shows the high-frequency region of the 442-nm spectrum. This wavelength is close to the B-band absorption of deoxyMb. It is therefore suited for detecting traces of this state. Indeed, the spectral analysis reveals significant contributions from well-known deoxyMb Raman lines, i.e., ν_2^D, ν_4^D, and ν_{11}^D. The deoxyMb modes arise from a combination of deoxyMb formed during irradiation of the sample with x-rays (Prusakov et al., 1995) and a fraction of the sample that is photodissociated during the measurement.

Fig. 3 *C* depicts the polarized spectra taken with 568-nm excitation. As in the case of spectra collected with 520-nm excitation (data not shown), asymmetrical heme modes of B_{1g}, A_{2g}, and even E_u symmetry are strongly excited by Q-state Jahn-Teller and interstate Herzberg-Teller coupling (Schweitzer-Stenner et al., 1997). The bands from high-frequency A_{1g}-type modes are comparatively weak, while A_{1g}-type modes of lower frequency (i.e., ν_5, ν_6) show considerable intensity. Interestingly, the band of the asymmetrical B_{1g}-type mode ν_{15} at 750 cm^{-1} is exceptionally intense. It also appears relatively strong in the B-band spectrum observed with 413-nm excitation.

The depolarization ratios, particularly of the A_{1g}-type modes, deviate dramatically from the expected value of 0.125, which is indicative of an unperturbed D_{4h} symmetry. This results in part from the fact that the sample itself was not totally optically clear. In this case the polarization of light is obfuscated by multiple scattering. However, this cannot explain the observation that some B_{1g} modes exhibit depolarization ratios lower than 0.75, particularly with 568-nm excitation, because the above contamination alone would cause ρ values between 0.75 and 1. Thus our data

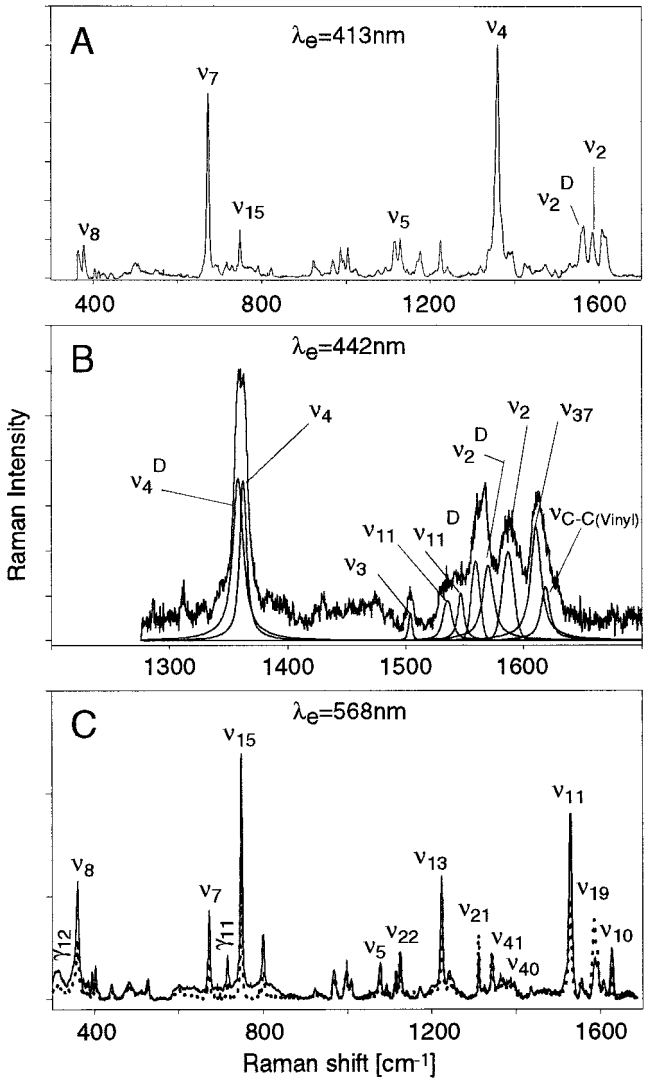

FIGURE 3 Resonance Raman spectra of the intermediate Fe(II)MbH_2O. (*A*) Unpolarized Raman spectrum taken with B-band excitation (413 nm). The most important bands are labeled by the mode notation of Abe et al. (1978). (*B*) High-frequency part of the unpolarized Raman spectrum measured with 442-nm excitation. The band profiles result from the spectral analysis described in the text. Raman bands labeled with the superscript D result from small amounts of Mbdeoxy or photodissociated H_2O. (*C*) polarized Raman spectra measured parallel (*solid line*) and perpendicular (*dotted line*) to the polarization of the incident laser beam with 568-nm excitation. The most intense bands are again labeled with Abe notation.

indicate a mixture of A_{1g}-type contributions to the Raman tensors of B_{1g} modes and B_{1g}-type contributions to the Raman tensors of A_{1g} modes, which both reflect the occurrence of B_{1g}-type distortions of the heme macrocycle (cf. Lemke et al., 1998).

The coupling constants S_{hj} for the modes ν_2, ν_4, ν_7, and ν_8 (corresponding to the label hj = 1, 2, 4, 5 used in Eq. 3) in the absorption-corrected 413-nm spectrum (Fig. 3 *A*) are listed in Table 3.

TABLE 2 Mode assignment and depolarization ratios of relevant bands observed in the Raman spectra of the intermediate Fe(II)MbH$_2$O shown in Fig. 3

Frequency (cm^{-1})	Assignment	ρ(413 nm)*	ρ(568 nm)
257	$\nu_9(A_{1g})$	—	0.55
307	$\gamma_7(A_{2u})$	—	0.50
316	$\gamma_{16}(B_{2u})$	—	0.51
359	$\nu_8(A_{1g})$	—	0.51
363	$\nu(C_\beta C_c C_d)_{prop}$	—	—
673	$\nu_7(A_{1g})$	0.52	0.46
750	$\nu_{15}(B_{1g})$	0.78	0.51
1114	$\nu_5(A_{1g})$	0.54	0.4
1124	$\nu_{22}(A_{2g})$	0.56	1.02
1223	$\nu_{13}(B_{1g})$	0.84	0.55
1312	$\nu_{21}(A_{2g})$	—	1.6
1343	$\nu_{41}(E_u)$	0.86	1.1
1362	$\nu_4(A_{1g})$	0.51	0.74
1504	$\nu_3(A_{1g})$	—	—
1532	$\nu_{11}(B_{1g})$	0.67	0.52
1586	$\nu_2(A_{1g})$	0.51	—
1588	$\nu_{19}(A_{2g})$	—	2.1
1618	$\nu(C{=}C)_{vinyl}$	0.53	—
1628	$\nu_{10}(B_{1g})$	—	0.66

*The depolarization ratio of the low-frequency modes could not be determined with sufficient accuracy.

Optical absorption spectra

The resolution of the vibronic structure in the optical spectra is limited by the homogenous bandwidth $\Gamma = 195$ cm^{-1}. Typical results of a least-squares fit of Eq. 2 to the experimental data are shown in Fig. 4. Fig. 4 *A* shows the 20 K spectrum of the first cycle, and Fig. 4 *B* shows the 150 K spectrum of the cycle to 180 K. The Soret band of the low temperature spectrum is very well described by the theory. The experimental data at 150 K show a clear deviation from the theoretical curve at the low-energy shoulder of the Soret band. The shoulder is a consequence of the spectral shift of deoxyMb and cannot be satisfactorily removed from all intermediate-state spectra. As done by other groups (Leone et al., 1996), the Lorentzian linewidth has been fixed at its low temperature value of $\Gamma = 195$ cm^{-1} for the whole temperature range. This procedure is also justified by the results of DiPace et al. (1992), who have shown for MbCO that Γ does not change in the temperature range below the glass transition of the solvent.

The temperature dependence of the electronic transition frequency, $\nu_0(T)$, of Fe(II)MbH$_2$O is displayed in Fig. 5 A. In all cases $\nu_0(T)$ is well defined if there is sufficient content of Fe(II)MbH$_2$O in the sample. Below 100 K, the shift is comparable to the shift observed in other myoglobin samples that are in a equilibrium state. Above 100 K, for the first series S1 Mbint150, the peak shifts strongly with temperature. For S1 Mbint170 and S1 Mbint180, the stronger temperature shift is only observable if the temperature range exceeded the range of the preceding series. There is no significant shift seen in the last data series.

With the exception of S_{h3}, the linear coupling constants are essentially temperature independent and do not change from one temperature series to the other. Therefore, they were averaged over all temperature cycles. The averages and their standard deviations are given in Table 3. The coupling constant of ν_{h3} at 1000 cm^{-1} shows qualitatively the same behavior as $\nu_0(T)$ of the intermediate state. Its value decreases in the first temperature cycle from the initial

TABLE 3 Averaged linear coupling constants for the different temperature cycles from the fit of the lineshape of the Soret band (except the mode at 1000 cm^{-1}) and the Raman spectra analysis

Mode, notation according to Eq. 3 Raman assignment	ν_{h1} ν_8	ν_{h2} ν_7	ν_{h3} ν_5	ν_{h4} ν_4	ν_{h5} ν_2
Fe(II)MbH$_2$O					
Frequency (cm^{-1})	372	673	1000	1362	1605
Coupling constants S_{hj} (opt)*	0.143 ± 0.026 (0.029)	0.047 ± 0.015 (0.015)	Changing	0.075 ± 0.006 (0.013)	0.026 ± 0.003 (0.013)
Coupling constants S_{hj} (Raman)	0.14 ± 0.02	0.10† ± 0.03	—	0.073 ± 0.03	0.013‡ ± 0.005
MbCO					
Frequency (cm^{-1})	350	676	1100	1374	—
Coupling constants S_{hj} (opt)	0.12 ± 0.02	0.06 ± 0.01	0.02 ± 0.008	0.09 ± 0.01	—
Deoxy Mb					
Frequency (cm^{-1})	370	674	1100	1357	—
Coupling constants S_{hj} (opt)	0.32 ± 0.02	0.24 ± 0.02	<0.01	0.10 ± 0.01	—

For comparison of the values for deoxy Mb and MbCO from Cupane et al. (1995) are also given.

*The values given in this row are the averaged values ± standard deviation from the mean value for the different temperature cycles. The value in parentheses is the error for a fit to a spectrum at 20 K.

†The higher coupling constant from the Raman measurement is probably caused by the amount of deoxy Mb present in the sample, as deoxy Mb has a much larger coupling constant than MbCO for the ν_7 band.

‡In our analysis of the Raman data we have only considered the intensity of the ν_2 band. Other weak modes may contribute to the somewhat larger effective coupling observed from the optical absorption data.

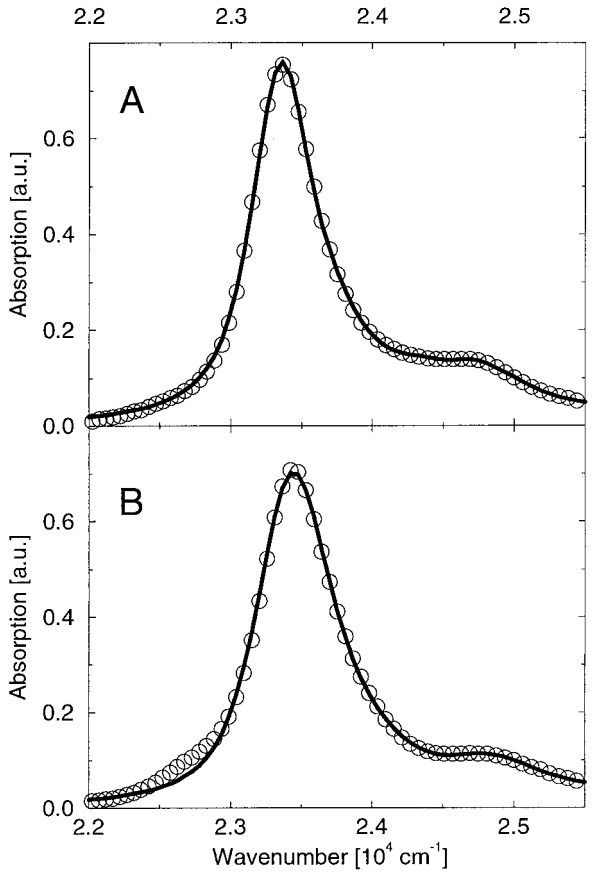

FIGURE 4 Spectra during the temperature cycles. (*A*) $T = 20$ K of the first series. (*B*) $T = 150$ K of the third series. *Circles*: Experimental points; *continuous lines*: fittings in terms of Eqs. 2, 3, and 4.

value of 0.065 to the final value of 0.02 and does not change during the following cycles. For comparison, the linear coupling constants obtained for MbCO and deoxyMb at 20 K by Cupane et al. (1995) are also included in Table 3.

Fig. 5 *B* shows the temperature dependence of $\sigma^2(T)$ as obtained from the evaluation of Eqs. 2, 3, and 4. Because all of the temperature cycles behave very similarly, the values of $\sigma^2(T)$ have been averaged at each temperature. For comparison the results for the equilibrium states MbCO and deoxyMb (from Cupane et al., 1995) are also shown. Because we are not interested in the different inhomogeneous broadening by the distribution of conformational substates, the curves for MbCO and deoxyMb have been shifted vertically to overlap with our experimental data at low temperatures.

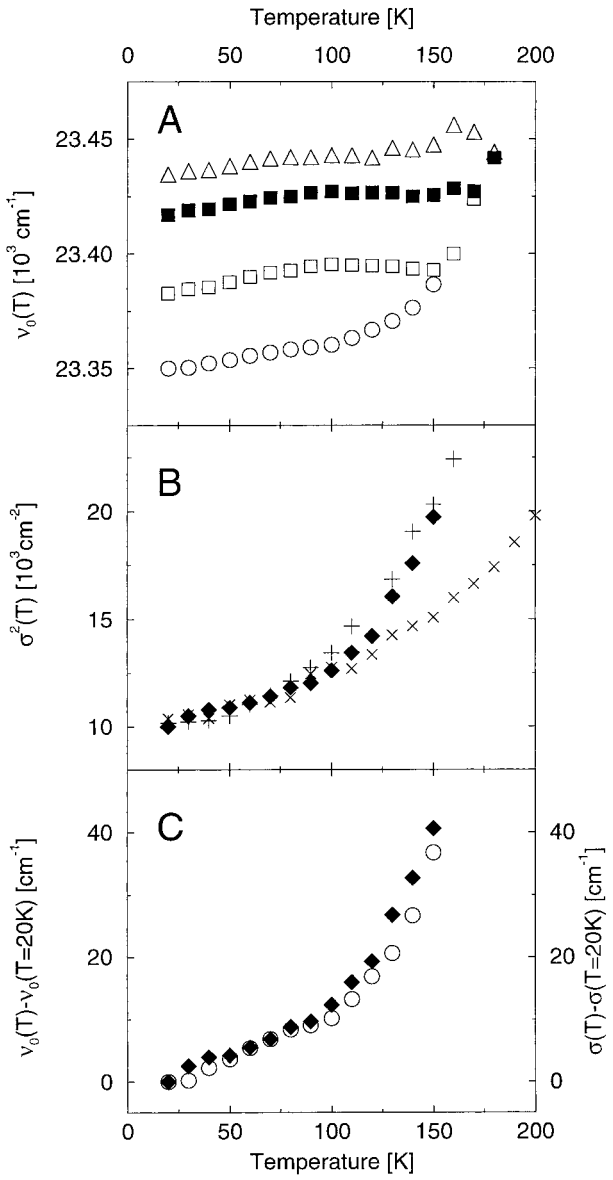

FIGURE 5 (*A*) Temperature dependence of the transition frequency ν_0 for the different temperature cycles. ○, Final temperature 150 K; □, final temperature 170 K; ■, final temperature 180 K; △, final temperature 200 K. (*B*) Averaged σ^2-values as a function of temperature (◆) in comparison with the values obtained for MbCO (×) and Mbdeoxy (+). (*C*) Comparison of the temperature dependence of the electronic transition frequency ($\nu_0(T) - \nu_0(T = 20$ K); ○) and the Gaussian broadening caused by the coupling to low-frequency modes (σ(T) − σ(T = 20 K); ◆).

DISCUSSION

Let us first consider the static structural properties of the intermediate state. The irradiation of the sample by light or x-rays at low temperatures results in a reduction of the heme iron, as suggested by Mössbauer spectroscopy (Parak and Prusakov, 1994; Prusakov et al., 1995). The iron becomes Fe(II) low-spin. The crystal structure clearly shows a sixth ligand (compare Fig. 2). Moreover, there are only minor structural changes.

This picture has to be slightly modified by the results of Raman spectroscopy. The Raman spectrum with excitation at 442 nm clearly shows contributions of a deoxyMb species. This is in agreement with earlier results obtained by

Mössbauer spectroscopy after x-ray reduction (Prusakov et al., 1995) and the photodissociation experiments of Lamb et al. (1998b). Before reduction, the metMb molecules are in a large number of conformational substates. Obviously, there are states where, after reduction, the barrier for the relaxation into the equilibrium deoxyMb state is so low that no metastable state can be seen on our time scale. In addition, a portion of the sample will be photodissociated by the excitation light. The sample for the Raman experiments has been warmed to 150 K. The x-ray structure was detected without illumination. The amount of deoxyMb found by Raman spectroscopy is on the border of the resolution limit of x-ray structure analysis.

The frequency positions of the spin marker bands ν_2 and ν_{19} (1586 and 1588 cm^{-1}) obtained from the spectra measured with 413- and 568-nm excitation are clearly diagnostic of a hexacoordinated low spin of the intermediate state. The ν_4 band was observed at 1362 cm^{-1}. This is generally indicative of a ferrous iron with a weak π-electron acceptor as the sixth ligand, as observed for various cytochromes, Fe(II)-protoporphyrins with two imidazoles or two CN ligands (Kitagawa et al., 1978; Choi et al., 1983).

The properties of the ν_4 mode deserve some further considerations. Its normal mode pattern is ascribable to an in-phase combination of $C_\alpha N$ and $C_\alpha C_\beta$ stretch (Li et al., 1990). This makes it sensitive to changes in the metal's oxidation and ligation states because both determine the extent of mixing between the d_π metal and the antibonding π^* orbital of the heme macrocycle (Kitagawa et al., 1978). A large mixing yields significant electron backbonding to the π^*-orbital, which shows considerable electron density in particular at the pyrrole nitrogens (Gouterman, 1959). This backbonding is strong only in the low-spin ferrous state, provided that the ligand has no significant π-electron acceptor capability (Spiro, 1983). We therefore conclude that the ν_4 frequency of 1362 cm^{-1} observed in the present study is diagnostic of π-electron back-donation from the iron's d_π into the e_g orbitals of the porphyrin ring. This notion is fully consistent with the behavior of ν_{10} and ν_{11}, which appear at 1628 cm^{-1} and 1532 cm^{-1}, significantly downshifted from their classical positions in spectra of low-spin hexacoordinated ferrous compounds (Spiro, 1983). As a consequence of the backbonding to the π^* orbital, the electronic ground state becomes more E_g-like, while it is generally A_{1g} for a perfectly neutral porphyrin (Gouterman, 1959). Thus the matrix elements of the electronic ground state with operators of B_{1g} symmetry lead to nonvanishing values and hence to a distortion of the ground-state potential (for a detailed discussion see Bersuker and Stavrov, 1988). This is also an explanation for the observed splitting of the Q-bands displayed in Fig. 1 *B*, which has already been attributed to a distortion of the heme group (Lamb et al., 1998a). The splitting for the B-bands is systematically smaller, as proved by Bersuker and Stavrov (1988); thus we were not able to detect it in the Soret spectra.

The lineshape of the Soret band of the intermediate state is at a glance a lot closer to the one observed for MbCO than the one observed for deoxyMb. Therefore, the formalism developed for a hexacoordinate heme was used for the evaluation of the lineshape (Cupane et al., 1995). The advantage of the present experiments is that the measurements are not limited to the fast rebinding processes, as is the case for Mb*CO, where the protein relaxation after photodissociation is only observable while the ligand is still unbound.

The high-frequency coupling constants were determined independently from the optical absorption measurements and Raman spectroscopy. They are in good agreement (compare Table 3). These coupling constants do not change during the temperature cycles, except for the mode ν_{h3} at 1000 cm^{-1}. Besides the Raman mode ν_5, the spectral region around 1000 cm^{-1} contains various intermediate and weak bands from stretching and rocking vibrations of the vinyl substituents (Hu et al., 1996). The intensity certainly depends on the substituents' orientation and their interaction with the protein. Hence, as this mode is affected by the relaxation within the intermediate state, it seems likely that small structural changes occur in the local heme environment that are just on the border of the resolution of the x-ray structure. The mode ν_7 ($= \nu_{h2}$) at 673 cm^{-1} is ascribed to a combination of $C_\alpha N$ stretch and $C_\alpha C_m C_\alpha$ bending (Li et al., 1990). Based on an analysis of the 10 K Mb*CO photoproduct Soret band, it has recently been suggested that its coupling strength increases with heme doming, which involves an out-of-plane displacement of the heme iron (Cupane et al., 1996b). The coupling constant for the mode ν_7 is relatively small and comparable to that obtained for MbCO (Table 3). It is considerably smaller than the corresponding value of deoxyMb. The similarity of the coupling constant for the ν_7 mode of Fe(II)MbH_2O and MbCO suggests a nearly in-plane position of the iron, in agreement with our x-ray results. The modes ν_{h1} and ν_{h4} show values close to the ones obtained for the fitting of the Soret band lineshape of MbCO and differ from those obtained for deoxyMb (see Table 3). It should be noted that the Lorentzian linewidth of the intermediate state is between those obtained for MbCO and deoxyMb (211 $\pm$ 7 cm^{-1} and 180 $\pm$ 10 cm^{-1} respectively; from Cupane et al., 1995).

The dynamics of the relaxation within the intermediate state is monitored by the electronic transition frequency $\nu_0(T)$. It changes steadily from one temperature cycle to the next. The temperature dependence of $\nu_0(T)$ obtained from the first cycle up to 150 K together with the ν_0 values of the other cycles at the highest temperature are in agreement with the previously published results (Lamb et al., 1998a), where only the position of the maximum of the Soret band was determined. Measuring different cycles clearly shows the relaxation character of this process. In succeeding cycles increasingly higher barriers can be overcome. In the last series no shift is observable; the variation results from the small amount of intermediate state still left in the sample,

especially above 150 K. Small structural changes influence the electrostatic interactions within the heme cavity affecting the π-electron system and thus the electronic transition frequency (Kushkuley and Stavrov, 1996). Franzen and Boxer (1997) discussed the spectral band shift of MbCO after photolysis in a similar way. Hence the electronic transition frequency monitors local changes in the heme environment of the intermediate state.

The recent publication of x-ray structures of metMb, MbO_2, MbCO, and deoxyMb at near-atomic resolution by Vojtechovsky et al. (1999) showed that there are only minor differences among the ligated structures. Even the differences between metMb and the ligated Fe^{2+} states MbCO and MbO_2 are small. This is in accordance with our findings that the structure of the intermediate state is close to the ligated Fe^{2+} states. An important difference between all ligated states and the unligated deoxyMb state is a shift of the heme. As deoxyMb is the final state after complete relaxation, the preceding relaxation within the intermediate could be a slight accommodation of the heme within the protein. A shift of the heme would result in a slightly altered environment and could thus be responsible for the shift in the electronic transition frequency.

Information about the dynamics of the intermediate state can be obtained from the width of the Gaussian broadening, $\sigma(T)$, which is caused by the coupling of the electronic transition to the bath of low-frequency vibrational modes. The width, $\sigma(T)$, is the same in each temperature cycle. In contrast to the electronic transition frequency, the Gaussian linewidth is not affected by the relaxation within the intermediate state. Obviously, the electronic transition frequency monitors small structural changes close to the heme, which change neither the low-frequency vibrational mode spectrum nor the coupling of the low-frequency modes to the electronic transition significantly.

The temperature dependence of $\sigma^2(T)$ for the intermediate state is much closer to the one observed for deoxyMb than to that for MbCO. Thus the low-frequency spectrum and the coupling to the low-frequency modes are similar for Fe(II)MbH_2O and deoxyMb. This is surprising, as the structure is close to that of MbCO. With respect to the low-frequency coupling, the metastable state shows already the behavior of the totally relaxed state. Note that a normal-mode analysis yields different results for the low-frequency spectrum of MbCO and deoxyMb (Melchers et al., 1996), as expected for different structures.

Comparing Fig. 5, *A* and *B*, one sees that the relaxation within the intermediate state monitored by the shift in the electronic transition frequency ν_0 occurs at a temperature similar to that at which the increase in $\sigma^2(T)$ occurs. A direct comparison of $\nu_0(T) - \nu_0(T = 20\ \mathrm{K})$ and $\sigma(T) - \sigma(T = 20\ \mathrm{K})$ is shown in Fig. 5 *C*. The temperature dependence of the shift of the fundamental electronic transition frequency of the Soret band correlates with the coupling to low-frequency modes. Thus the increased coupling to low-frequency modes may be required for the relaxation within the intermediate state to proceed significantly.

CONCLUSION

After the low-temperature reduction of metMb, the molecules relax in two main steps into the equilibrium deoxyMb structure. We have characterized an intermediate state with a six-ligated Fe(II) low-spin heme and a structure very similar to those of metMb or MbCO. Within the intermediate state, relaxations occur with increasing temperature as precursors of the relaxation to the deoxyMb conformation. The shift in the transition frequency could be an adjustment of the heme with respect to the protein backbone.

Whereas all of the static properties of Mbint are close to those of hexaligated Fe(III) or Fe(II) myoglobin, the dynamic behavior shows strong similarities to that of deoxyMb. This is seen from the temperature dependence of σ^2. Comparing these features, we come to the following picture: at low temperatures the protein configuration is frozen. No structural relaxation into the deoxyMb equilibrium state can follow after flash photolysis of the water molecule. It rebinds with an enthalpy distribution similar to that for CO and O_2 rebinding. The six-coordinated structure of the heme iron is stable. However, relaxation within the intermediate state occurs, driven by the low-frequency dynamics of the active site. The similarity of the dynamic properties of Mbint and deoxyMb make Mbint less and less stable with increasing temperature. If the temperature becomes high enough to allow global structural relaxations (typically around $T = 180$ K), the water molecule can be shaken off and cannot rebind, and the structure relaxes to deoxyMb. Here we have clear differences in the behavior of the CO ligand. This molecule has to be photodissociated and it can rebind. However, the relaxation process into the deoxy structure after the sixth ligand has left its coordination is probably the same.

This work was supported by the Deutsche Forschungsgemeinschaft (SFB-533, contract 436 RUS 113/414), the Russian Foundation of Basic Research (grants 98-04-04101 and 99-04-48208 to VEP), and the Fonds der Chemie. DCL gratefully acknowledges support from the Alexander von Humboldt Foundation. We thank Prof. Wolfgang Dreybrodt for his very useful suggestions for the experimental setup of the Raman measurements and his general support of the project.

REFERENCES

Abe, M., T. Kitagawa, and Y. Kyogoku. 1978. Resonance Raman spectra in octaethylporphyin-Ni(II) and mesodeuterated and ^{15}N substituted derivatives. II. A normal coordinate analysis. *J. Chem. Phys.* 69: 4526–4534.

Agmon, N., and J. J. Hopfield. 1983. CO binding to heme proteins: A model for barrier height distributions and slow conformational changes. *J. Chem. Phys.* 79:2042–2053.

Austin, R. H., K. W. Beeson, L. Eisenstein, H. Frauenfelder, and I. C. Gunsalus. 1975. Dynamics of ligand binding to myoglobin. *Biochemistry.* 14:5355–5373.

Balasubramanian, S., D. G. Lambright, M. C. Marden, and S. G. Boxer. 1993. CO recombination to human myoglobin mutants in glycerol-water solutions. *Biochemistry.* 32:2202–2212.

Bersuker, I. B., and S. S. Stavrov. 1988. Structure and properties of metalloporphyrins an hemoproteins: the vibronic approach. *Coord. Chem. Rev.* 88:1–68.

Brünger, A. T. 1992. X-PLOR, version 3.1. A System for X-Ray Crystallography and NMR. Yale University Press, New Haven, CT.

CCP4. 1994. Collaborative computational project, number 4. *Acta Crystallogr. D.* 50:760–763.

Chan, C. K., and J. B. Page. 1983. Temperature effects in the time correlator theory of resonance Raman scattering. *J. Chem. Phys.* 79: 5234–5250.

Chan, C. K., and J. B. Page. 1984. T ≠ 0 K multimode modeling of optical absorption spectra and resonance Raman profiles. *Chem. Phys. Lett.* 104:609–614.

Choi, S., J. J. Lee, Y. H. Wie, and T. G. Spiro. 1983. Resonance Raman and electronic spectra of heme a complexes and cytochrome oxidase. *J. Am. Chem. Soc.* 105:3692–3707.

Cupane, A., M. Leone, L. Cordone, H. Gilch, W. Dreybrodt, E. Unger, and R. Schweitzer-Stenner. 1996a. Conformational properties of Ni(II)octaethylporphyrin in solution. 2. A low-temperature optical absorption spectroscopy study. *J. Phys. Chem.* 100:14192–14197.

Cupane, A., M. Leone, E. Vitrano, and L. Cordone. 1995. Low temperature optical absorption spectroscopy: an approach to the study of stereodynamic properties of hemeproteins. *Eur. Biophys. J.* 23:385–398.

Cupane, A., E. Vitrano, P. Ormos, and G. U. Nienhaus. 1996b. Heme geometry in the 10 K photoproduct from sperm whale carbonmonoxymyoglobin. *Biophys. Chem.* 60:111–117.

DiPace, A., A. Cupane, M. Leone, E. Vitrano, and L. Cordone. 1992. Protein dynamics vibrational coupling, spectral broadening mechanisms, and anharmonicity effects in carbonmonoxy heme proteins studied by the temperature dependence of the Soret band line shape. *Biophys. J.* 63:475–484.

Esquerra, R. M., R. A. Goldbeck, D. B. Kim-Shapiro, and D. S. Kliger. 1998. Spectroscopic evidence for nanosecond protein relaxation after photodissociation of myoglobin-CO. *Biochemistry.* 37:17527–17536.

Franzen, S., and S. G. Boxer. 1997. On the origin of heme absorption band shifts and associated protein structural relaxation in myoglobin following flash photolysis. *J. Biol. Chem.* 272:9655–9660.

Gouterman, M. 1959. Study of the effects of substitution on the absorption spectra of porphyrin. *J. Chem. Phys.* 30:1139–1161.

Hartmann, H., S. Zinser, P. Komninos, R. T. Schneider, G. U. Nienhaus, and F. Parak. 1996. X-ray structure determination of a metastable state of carbonmonoxy myoglobin after photodissociation. *Proc. Natl. Acad. Sci. USA.* 93:7013–7016.

Hodel, A., S.-H. Kim, and A. T. Brünger. 1992. Model bias in macromolecular crystal structures. *Acta Crystallogr. A.* 48:851–859.

Hu, S., K. M. Smith, and T. G. Spiro. 1996. Assignment of protoheme resonance Raman spectrum by heme labeling in myoglobin. *J. Am. Chem. Soc.* 118:12638–12646.

Jentzen, W., E. Unger, G. Karvounis, J. A. Shelnutt, W. Dreybrodt, and R. Schweitzer-Stenner. 1995. Conformational properties of nickel(II)octaethylporphyrin in solution. 1. Resonance excitation profiles and temperature dependence of structure sensitive Raman lines. *J. Phys. Chem.* 100:14184–14191.

Johnson, J. B., D. C. Lamb, H. Frauenfelder, J. D. Müller, B. McMahon, G. U. Nienhaus, and R. D. Young. 1996. Ligand binding to heme proteins. VI. Interconversion of taxonomic substates in carbonmonoxymyoglobin. *Biophys. J.* 71:1563–1573.

Kitagawa, T., Y. Ozaki, and Y. Kyogoku. 1978. Resonance Raman studies on the ligand-iron interactions in hemoproteins and metallo-porphyrins. *Adv. Biophys.* 11:153–196.

Kleinert, T., W. Doster, H. Leyser, W. Petry, V. Schwarz, and M. Settles. 1998. Solvent composition and viscosity effects on the kinetics of CO binding to horse myoglobin. *Biochemistry.* 37:717–733.

Kushkuley, B., and S. Stavrov. 1996. Theoretical study of the distal-side steric and electrostatic effects on the vibrational characteristics of the FeCO unit of the carbonylheme proteins and their models. *Biophys. J.* 70:1214–12229.

Lamb, D. C., A. Ostermann, V. E. Prusakov, and F. G. Parak. 1998a. From metmyoglobin to deoxy myoglobin: relaxations of an intermediate state. *Eur. Biophys. J.* 27:113–125.

Lamb, D. C., V. E. Prusakov, N. Engler, A. Ostermann, P. Schellenberg, F. G. Parak, and G. U. Nienhaus. 1998b. Photodissociation and rebinding of H_2O to ferrous sperm whale myoglobin. *J. Am. Chem. Soc.* 120:2981–2982.

Lambright, D. G., S. Balasubramanian, and S. G. Boxer. 1991. Protein relaxation dynamics in human myoglobin. *Chem. Phys.* 158:249–260.

Lemke, C., W. Dreybrodt, J. A. Shelnutt, J. M. E. Quirke, and R. Schweitzer-Stenner. 1998. Polarized Raman dispersion spectroscopy probes planar and non-planar distortions of Ni(II)porphyrins with different peripheral substituents. *J. Raman Spectrosc.* 29:945–953.

Leone, M., A. Cupane, and L. Cordone. 1996. Low temperature optical spectroscopy of low-spin ferric hemeproteins. *Eur. Biophys. J.* 24: 117–124.

Li, X. Y., R. S. Czernuszewicz, J. R. Kincaid, P. Stein, and T. G. Spiro. 1990. Consistent porphyrin force field. 2. Nickel octaethylporphyrin skeletal and substituent mode assignment from ^{15}N, meso-d_4, and methylene-d_{16} Raman and infrared isotope shifts. *J. Phys. Chem.* 94:47–61.

Lim, M., T. A. Jackson, and P. A. Anfinrud. 1993. Nonexponential protein relaxation: dynamics of conformational change in myoglobin. *Proc. Natl. Acad. Sci. USA.* 90:5801–5804.

Makinen, M. W., and A. K. Churg. 1983. Structural and analytical aspects of the electronic spectra of hemeproteins. *In* Iron Porphyrins, Part I. A. B. P. Lever and H. B. Gray, editors. Addison-Wesley, Reading, PA. 141–235.

Melchers, B., E. W. Knapp, F. Parak, L. Cordone, A. Cupane, and M. Leone. 1996. Structural Fluctuations of Myoglobin from Normal-Modes, Mössbauer, Raman and Absorption Spectroscopy. *Biophys. J.* 70:2092–2099.

Nienhaus, G. U., J. R. Mourant, and H. Frauenfelder. 1992. Spectroscopic evidence for conformational relaxation in myoglobin. *Proc. Natl. Acad Sci. USA.* 89:2902–2906.

Ormos, P., S. Szaraz, A. Cupane, and G. U. Nienhaus. 1998. Structural factors controlling ligand binding to myoglobin: a kinetic hole burning study. *Proc. Natl. Acad. Sci. USA.* 95:6762–6767.

Parak, F., H. Hartmann, K. D. Aumann, H. Reuscher, G. Rennekamp, H. Bartunik, and W. Steigemann. 1987. Low temperature x-ray investigation of structural distributions in myoglobin. *Eur. Biophys. J.* 15: 237–249.

Parak, F., and V. E. Prusakov. 1994. Relaxation of non-equilibrium states of myoglobin studied by Mössbauer spectroscopy. *Hyperfine Interact.* 91:885–890.

Perutz, M. F., A. J. Wilkinson, M. Paoli, and G. G. Dodson. 1998. The stereochemical mechanism of the cooperative effects in hemoglobin revisited. *Annu. Rev. Biophys. Biomol. Struct.* 27:1–34.

Prusakov, V. E., J. Steyer, and F. Parak. 1995. Mössbauer spectroscopy on nonequilibrium states of myoglobin: a study of r-t relaxation. *Biophys. J.* 68:2524–2530.

Read, R. J. 1986. Improved Fourier coefficients for maps using phases from partial structure with errors. *Acta Crystallogr. A.* 42:140–149.

Schlichting, I., J. Berendzen, G. N. Phillips, Jr., and R. M. Sweet. 1994. Crystal structure of photolysed carbonmonoxy-myoglobin. *Nature.* 371: 808–812.

Schweitzer-Stenner, R. 1989. Allosteric linkage-induced distortions of the prosthetic group in haem proteins as derived by the theoretical interpretation of the depolarization ratio in resonance Raman scattering. *Q. Rev. Biophys.* 22:381–479.

Schweitzer-Stenner, R., A. Stichternath, W. Dreybrodt, W., Jentzen, X.-Z. Song, J. A. Shelnutt, O. Faurskov-Nielsen, C. J. Medforth, and K. M.

Smith. 1997. Raman dispersion spectroscopy on the highly saddled nickel(II)-octaethyltetraphenylporphyrin reveals the symmetry of nonplanar distortions and the vibronic coupling strength of normal modes. *J. Chem. Phys.* 107:1794–1814.

Smulevich, G., S. Hu, K. R. Rodgers, D. B. Goodin, K. M. Smith, and T. G. Spiro. 1996. Heme-protein interactions in cytochrome *c* peroxidase revealed by site-directed mutagenesis and resonance Raman spectra of isotopically labelled hemes. *Biospectroscopy.* 2:365–376.

Spiro, T. G. 1983. The resonance Raman spectroscopy of metallo porphyrins and heme proteins. *In* Iron Porphyrins, Part II. A. B. P. Lever and H. B. Gray, editors. Addison-Wesley, Reading, PA. 90–159.

Šrajer, V., K. T. Schomacker, and P. M. Champion. 1986. Spectral broadening in biomolecules. *Phys. Rev. Lett.* 57:1267–1270.

Šrajer, V., and P. M. Champion. 1991. Investigations of optical line shapes and kinetic hole burning in myoglobin. *Biochemistry.* 30:7390–7402.

Šrajer, V., T.-Y. Teng, T. Ursby, C. Pradervand, Z. Ren, S.-I. Adachi, W. Schildkamp, D. Bourgeois, M. Wulff, and K. Moffat. 1996. Photolysis of the carbon monoxide complex of myoglobin: Nanosecond time-resolved crystallography. *Science.* 274:1726–1729.

Steinbach, P. J., A. Ansari, J. Berendzen, D. Braunstein, K. Chu, B. R. Cowen, D. Ehrenstein, H. Frauenfelder, B. Johnson, D. C. Lamb, S. Luck, J. R. Mourant, G. U. Nienhaus, P. Ormos, R. Phillip, A. Xie, and R. D. Young. 1991. Ligand binding to heme proteins: connection between dynamics and function. *Biochemistry.* 30:3988–4001.

Teng, T.-Y., V. Šrajer, and K. Moffat. 1994. Photolysis-induced structural changes in single crystals of carbonmonoxy myoglobin at 40 K. *Nature Struct. Biol.* 1:701–705.

Vitkup, D., G. A. Petsko, and M. Karplus. 1997. A comparison between molecular dynamics and x-ray results for dissociated CO in myoglobin. *Nature Struct. Biol.* 4:202–208.

Vojtechovsky, J., K. Chu, J. Berendzen, R. M. Sweet, and I. Schlichting. 1999. Crystal structures of myoglobin-ligand complexes at near-atomic resolution. *Biophys. J.* 77:2153–2174.

Zgierski, M. Z., and M. Pawlikowski. 1982. Depolarization dispersion curves of resonance Raman fundamentals of metalloporphyrins and metallophtalocyanines. Subject to asymmetric perturbations. *Chem. Phys.* 65:335–367.